Astron. Astrophys. 331, 894–900 (1998)

ASTRONOMY AND ASTROPHYSICS

Optical and NIR modelling of NGC 891

E.M. Xilouris[1,3], P.B. Alton[4], J.I. Davies[4], N.D. Kylafis[2,3], J. Papamastorakis[2,3], and M. Trewhella[4]

[1] University of Athens, Department of Physics, Section of Astrophysics, Astronomy & Mechanics, GR-157 83 Athens, Greece
[2] University of Crete, Physics Department, P.O. Box 2208, GR-710 03 Heraklion, Crete, Greece
[3] Foundation for Research and Technology-Hellas, P.O. Box 1527, GR-711 10 Heraklion, Crete, Greece
[4] Department of Physics and Astronomy, University of Wales, Cardiff, P.O. Box 913, Cardiff CF2 3YB, UK

Received 12 September 1997 / Accepted 13 November 1997

Abstract. We compare B, V, I, J, K surface photometry of the edge-on spiral galaxy NGC 891 with corresponding surface photometry calculated from a realistic model of spiral galaxies, taking into account both absorption and scattering by dust. For the stars and the dust in the disk, we use exponential distributions in both directions, radially and perpendicular to the plane of the disk. For the bulge we use the emissivity distribution given by the Hubble profile. Apart from the exponential main stellar disk, it was found necessary to include also a second stellar disk, describing the young stellar population in this galaxy. This disk has a scaleheight about three times less than that of the main disk and its emissivity is constant in the radial direction with a cut off at the visual end of the galaxy. The young stars are detected only in the B and V bands, indicating that in these bands they contribute significantly to the light near the major axis. For this galaxy we have found a face-on central optical depth of less than one in all bands, indicating that if the galaxy were seen face-on, it would be transparent in the optical and near infrared region of the spectrum. The total dust mass is calculated from the model parameters and the gas to dust ratio is found to be very similar to that of our Galaxy. The ratios A_λ/A_V of the extinction values are computed for the five bands and compare quite well with the values given for our Galaxy.

Key words: galaxies: photometry – galaxies: spiral – galaxies: individual: NGC 891 – galaxies: ISM – dust, extinction – galaxies: structure

1. Introduction

In our attempt to help answer the difficult question of whether spiral galaxies are opaque or not, we have initiated a program to study the distribution of stars and dust in the nearby, well resolved galaxies.

Send offprint requests to: xilouris@physics.uch.gr

In the first paper of this series (Xilouris et al. 1997, hereafter Paper I), a detailed modelling of the late-type spiral galaxy UGC 2048 was done, using observations in the B, V, I bands and the radiative transfer model described in Kylafis & Bahcall (1987, hereafter KB87). The main conclusion from that study was that UGC 2048 would be optically thin throughout its surface, if it were to be seen face-on. In the present work, we continue our study by modelling the well-known spiral galaxy NGC 891, not only in the B, V, I optical bands, but also in the J and K near infrared bands.

Several studies dealing with two-dimensional decomposition of this galaxy have been reported (e.g., van der Kruit & Searle 1981; Bahcall & Kylafis 1985; Shaw & Gilmore 1989). In these studies, photometric parameters are derived by fitting various stellar models to the surface brightness of the galaxy in parts away from the dust lane. All of these studies suggest that NGC 891 could be fitted by a two-stellar-component model consisting either of a thin disk (with exponential or sech^2z type functions) and an $R^{1/4}$ law profile, or a thin disk and a thick disk, the second component being responsible for the distribution of population II stars. When the dust is included however, things become more complicated and a 3D radiative transfer model is needed. KB87 used such a model to interpret F-band data. Two disks, exponential in the radial direction and sech^2z in the vertical direction were used to describe the stellar and dust distributions and a fit to the surface brightness of the galaxy was done in several parts of the galaxy. The work that will be presented in this paper is complementary to that of KB87 in the sense that the model is extended to the five bands mentioned above and also a more complete model, including a bulge component, is used for a global fit to the surface brightness of the galaxy.

In Sect. 2 we describe the observations and the data reduction, in Sect. 3 we present the model that we have used, in Sect. 4 we fit the model to the real data, in Sect. 5 we draw our conclusions and a brief summary is presented in Sect. 6.

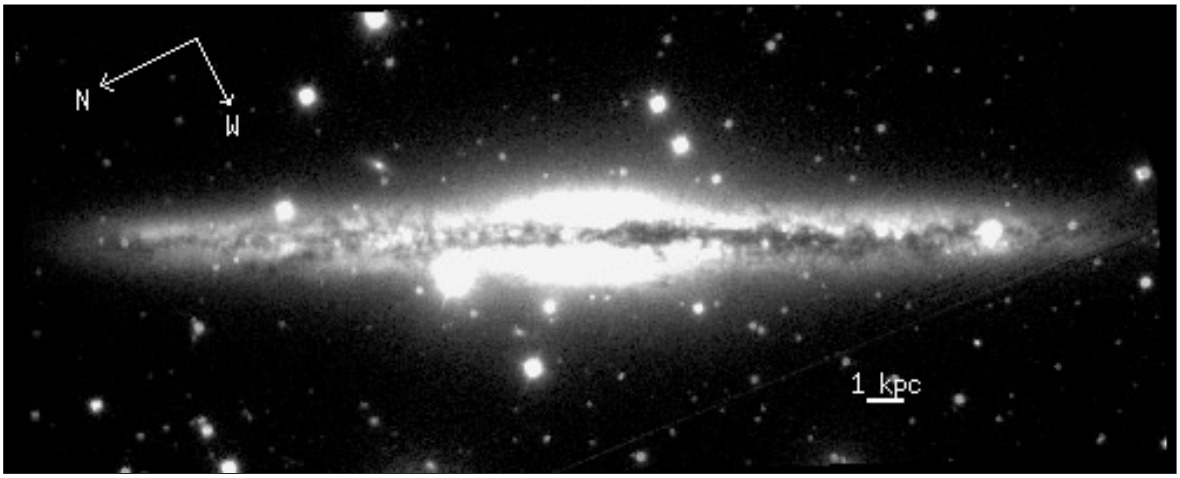

Fig. 1. An 80 min exposure of NGC 891 in the B-band.

2. Observations and data reduction

Observations of the optical images were made on October 16, 1996 with the 1.3 m telescope at Skinakas Observatory in Crete. The telescope, an $f/7.7$ Ritchey-Cretien, was equiped with a focal reducer, producing an enlargement of the field of view by a factor of 1.9, and with a Thomson 1024×1024 CCD camera with 19μm pixels. This arrangement produces a scale of 0.75 arcsec/pixel and a field of view of approximately $13' \times 13'$. Assuming a distance of 9.5 Mpc for NGC 891 (van der Kruit & Searle 1981), the pixel size corresponds to 34 pc. The B and V passbands that we use are comparable to those of Johnson's photometric system with effective wavelengths 0.443 μm and 0.564 μm respectively, while the I passband is comparable to that of Cousin's photometric system, with effective wavelength 0.809 μm. In order to calibrate the images, we used standard stars and a photometric procedure described in detail in Paper I. The rms deviations from the least squares fit between catalogue magnitudes and calibrated magnitudes for the standard stars were 0.03 mags in B, 0.02 mags in V and 0.03 mags in I. The total integration time was 80 min in B, 20 min in V and 20 min in I. The seeing was measured to be $1.4''$ for that night.

Observations of the NIR images were made on November 1995 using the 2.5 m telescope at the Wyoming Infrared Observatory (WIRO). The detector that was used was a Michigan Infrared Camera (MIRC) with a NICMOS II 128×128 chip. The pixel size at the prime focus was $2.23''$ which at the distance of 9.5 Mpc corresponds to 0.102 kpc. A mosaic of three frames was made for each band (J and K) and the total integration time was 18 mins for each filter. During the observations, "blank sky" frames were taken at frequent intervals and then subtracted after bias and flatfield correction. Calibration of the NIR images was done using the aperture photometry of Aaronson (1977).

Standard photometric procedures were used (described in more detail in Paper I) in order to reduce the images in a way suitable for the model.

3. Model

NGC 891 (often quoted to be very similar to our own Galaxy) is an Sb Hubble type galaxy, seen almost edge-on. The relatively small distance (9.5 Mpc) to this galaxy, gives us an advantage of high-resolution imaging, revealing many details of the distribution of light and dust.

Considered to be an example of a typical spiral galaxy, NGC 891 is expected to consist of a central bulge (mainly populated by old stars) and a disk formed by a mixture of stars and interstellar dust and gas, organized in spiral formations. The projection of such a system on the sky, with the plane of the disk almost parallel to our line of sight, results in a surface brightness distribution like that shown in Fig. 1. Neglecting for the moment the small scale structure and clumpiness, one can distinguish three main components in the projected image. A stellar disk, a dust lane (located along the major axis of the disk) and a bulge in the central region of the galaxy. Even though the detailed spiral structure of the galaxy is not known and may be quite complicated on small scales, it is possible to use simple mathematical functions to obtain an "on average" description of the galaxy. The successful modelling that was done on UGC 2048 (Paper I), encourages us to do the same to NGC 891. It is obvious though that studying galaxies in various orientations, which is something we intend to do, will allow for a better comprehension of the general opacity problem.

Thus, for the stellar distribution in the disk, we use exponential functions in both the radial and the vertical direction with respect to the plane of the disk i.e.,

$$L_{disk}(R,z) = L_s \exp\left(-\frac{R}{h_s} - \frac{|z|}{z_s}\right). \quad (1)$$

Here R and z are the cylindrical coordinates, L_s is the stellar emissivity at the center of the disk and h_s and z_s are the scale-length and scaleheight respectively of the stars in the disk. The

central surface brightness of such a distribution, assuming that the galaxy is seen edge-on is given by

$$I_s = 2L_s h_s. \quad (2)$$

For a detailed description of all the parameters, the reader should refer to Sect. 4 of Paper I.

For the stellar emissivity in the bulge, both the Hubble profile (Hubble 1930) and the $R^{1/4}$ law (de Vaucouleurs 1953) provide an excellent fit. As mentioned in Paper I, the parameters describing the stellar disk are not affected significantly by the type of bulge used. Thus, we use the Hubble profile, the emissivity of which is given by

$$L_{bulge} = L_b(1 + B^2)^{-3/2}, \quad (3)$$

where L_b is the emissivity of the bulge at the center and

$$B = \frac{\sqrt{R^2 + z^2(b/a)^2}}{R_e}, \quad (4)$$

with R_e being the effective radius of the bulge and a and b the semi-major and semi-minor axis respectively. The central value of the bulge surface brightness, if the model galaxy is seen edge-on, is

$$I_b = 2L_b R_e. \quad (5)$$

The total stellar emissivity is then given by

$$L(R, z) = L_{disk}(R, z) + L_{bulge}(R, z). \quad (6)$$

For the extinction coefficient we use a double exponential law, namely

$$\kappa_\lambda(R, z) = \kappa_\lambda \exp\left(-\frac{R}{h_d} - \frac{|z|}{z_d}\right), \quad (7)$$

where κ_λ is the extinction coefficient at wavelength λ at the center of the disk and h_d and z_d are the scalelength and scale-height respectively of the dust. The central optical depth of the model galaxy seen face-on is

$$\tau_\lambda^f = 2\kappa_\lambda z_d. \quad (8)$$

The model that we have used is that described in KB87 (see also Paper I). A Henyey-Greenstein phase function has been used for the scattering of the dust (Henyey & Greenstein 1941). The values for the anisotropy parameter g and the albedo ω have been taken from Bruzual et al. (1988). Our task is to find those values of the parameters in Eqs. (1) - (8) which create images of the model galaxy as close as possible to the images of the observed galaxy.

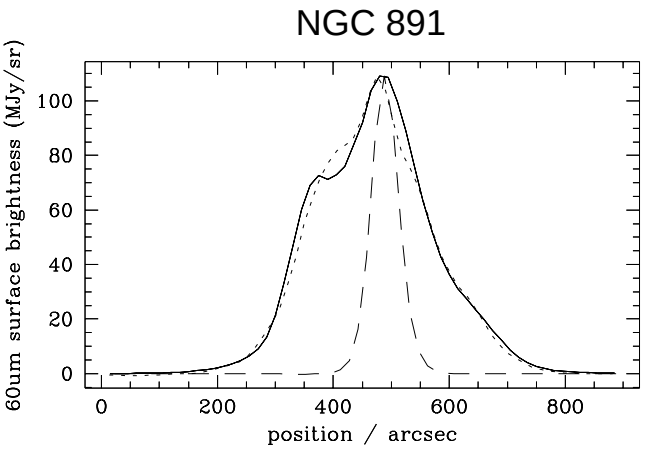

Fig. 2. Average surface brightness profiles for the 60μm (solid line) and the 20 cm radio continuum emission (dotted line) along the major axis of NGC 891. The dashed line traces the surface brightness of the IRAS beam.

4. Model fitting

A more careful examination of the galaxy image, especially in the B-band (Fig. 1), shows an asymmetry between the left (northern) and the right (southern) halves. This asymmetry appears in the dust lane, with the left half being brighter than the right one. This extra brightness of the left part is believed to be due to the presence of young OB stars. As already mentioned by van der Kruit & Searle (1981; see also Wainscoat et al. 1987), what seems to happen is that the spiral arm in the left half is approaching, with the dust trailing the arms. The young stars form H_{II} regions in front of the dust, thus resulting in an excess of light. Exactly the opposite happens in the right half of the galaxy, where the spiral arm is now receding, with the young stars hidden behind the dust and as a result the light of these stars is absorbed. This is evident in the B and V bands. FIR and radio continuum data also support the idea of the existence of star forming regions in the galaxy. This is shown in Fig. 2 (courtesy of Alton et al. 1997) where average surface brightness profiles along the major axis of the galaxy for 60μm (solid line) and 20 cm continuum (dotted line) are plotted. The dashed line traces the surface brightness of the IRAS beam. From this plot it is seen that there is an excess of FIR and radio emission which is very obvious in the left (northern) part of the galaxy while it is less evident in the right (southern) part. The region where we see this extra emission coinsides with the part of the galaxy which is brighter in the optical (see Fig. 1) and believed to be due to the existence of young stars. Because our model is not yet able to take into account any azimuthal structure, we folded the image so that the fitted galaxy is an average of the left and right halves of the galaxy. This method worked quite well for UGC 2048 (see Paper I) where "average" stellar and dust components were calculated.

Our first attempt to fit the data with the distributions described above was successful for the I, J, K bands. In these bands we had excellent agreement between the real galaxy im-

Table 1. Global model fit parameters for NGC 891.

Parameter	Units	K band		J band		I band		V band		B band	
I_s	mags/arcsec^2	15.40	$\pm$0.04	15.88	$\pm$0.06	17.39	$\pm$0.05	18.87	$\pm$0.07	19.75	$\pm$0.05
z_s	kpc	0.32	$\pm$0.01	0.38	$\pm$0.01	0.37	$\pm$0.01	0.39	$\pm$0.01	0.40	$\pm$0.01
h_s	kpc	3.93	$\pm$0.1	3.90	$\pm$0.2	4.92	$\pm$0.1	5.71	$\pm$0.2	5.80	$\pm$0.1
I_b	mags/arcsec^2	14.80	$\pm$0.05	16.11	$\pm$0.08	16.27	$\pm$0.04	17.12	$\pm$0.06	18.87	$\pm$0.09
R_e	kpc	0.24	$\pm$0.02	0.37	$\pm$0.05	0.41	$\pm$0.02	0.34	$\pm$0.04	0.48	$\pm$0.05
b/a	–	0.75	$\pm$0.02	0.82	$\pm$0.01	0.54	$\pm$0.01	0.55	$\pm$0.01	0.55	$\pm$0.01
τ_λ^f	–	0.09	$\pm$0.01	0.22	$\pm$0.01	0.47	$\pm$0.01	0.70	$\pm$0.01	0.78	$\pm$0.01
z_d	kpc	0.22	$\pm$0.02	0.25	$\pm$0.01	0.24	$\pm$0.01	0.26	$\pm$0.01	0.32	$\pm$0.02
h_d	kpc	8.41	$\pm$0.3	8.41	$\pm$0.4	7.34	$\pm$0.4	8.10	$\pm$0.2	8.01	$\pm$0.2
θ	degrees	89.6	$\pm$0.1	89.6	$\pm$0.1	89.7	$\pm$0.1	89.8	$\pm$0.2	89.8	$\pm$0.2

Table 2. Global model fit parameters for NGC 891 in V and B bands using a second stellar disk.

Parameter	Units	V band		B band	
I_s	mags/arcsec^2	18.81	$\pm$0.05	19.90	$\pm$0.04
z_s	kpc	0.39	$\pm$0.01	0.41	$\pm$0.01
h_s	kpc	5.36	$\pm$0.2	5.90	$\pm$0.2
I_b	mags/arcsec^2	17.25	$\pm$0.04	19.15	$\pm$0.04
R_e	kpc	0.38	$\pm$0.04	0.71	$\pm$0.05
b/a	–	0.51	$\pm$0.01	0.45	$\pm$0.01
τ_λ^f	–	0.72	$\pm$0.01	0.86	$\pm$0.01
z_d	kpc	0.28	$\pm$0.02	0.31	$\pm$0.02
h_d	kpc	7.75	$\pm$0.3	8.39	$\pm$0.3
θ	degrees	89.8	$\pm$0.2	89.8	$\pm$0.2
I_{OB}	mags/arcsec^2	20.76	$\pm$0.02	20.25	$\pm$0.07
z_{OB}	kpc	0.15	$\pm$0.01	0.15	$\pm$0.01

Table 3. Percentage coverage of the residuals throughout the galaxy's image.

Band	$< 10\%$	$< 20\%$	$< 30\%$	$< 40\%$	$< 50\%$
B	42.0%	67.4%	82.2%	89.4%	93.1%
V	48.9%	72.6%	85.3%	92.3%	95.1%
I	49.7%	77.2%	88.4%	92.2%	95.9%
J	36.2%	63.5%	82.3%	91.8%	96.0%
K	34.4%	62.6%	81.5%	94.0%	99.3%

age and the model image that we created. For the B and V bands though, the fit was poor, giving high residuals between model and data. Furthermore, the stellar scalelength took values three or four times larger than those derived from the I, J and K bands. All these effects were the result of the young stars in the galactic plane, which contribute to the surface brightness along the major axis of the galaxy and make the exponential disk insufficient to describe both the main stellar population in the disk and the young stars. To overcome this problem (at least temporarily) we were led to model only the right half of the galaxy in the B and V bands which is "well behaved" (i.e. the dust lane is not perturbed by any clump of young stars, but instead it is clearly detected throughout the galaxy's major axis). In a later stage however (see end of this section), we did model the folded B and V images of the galaxy by introducing an additional stellar disk to describe the young stellar population.

As we did in Paper I, a global least squares fit of the model to the observed data is performed. For the fit, the Levenberg-Marquardt algorithm is used and the inverse Student's t distribution function is used to calculate the 95% confidence interval on the regression parameters. Both of these algorithms are embedded in the IMSL MATH/LIBRARY.

The full set of the parameters that are directly derived from the fit and are needed to describe the model galaxy are a) the central edge-on surface brightness I_s of the disk with the scaleheight z_s and scalelength h_s, b) the central edge-on surface brightness of the bulge I_b, with the effective radius R_e and the ellipticity b/a, c) the central face-on optical depth τ_λ^f with scaleheight z_d and scalelength h_d for the dust and finally d) the inclination angle θ. As we described in Paper I, some preliminary values for the parameters are first derived by partial fitting techniques. The final values derived from the global fit are given in Table 1. In this table, the central edge-on surface brightness I_s of the main disk and of the bulge I_b are given in units of mags/arcsec^2, while all lengths are given in kpc.

As mentioned before, our difficulties in modelling the B and V folded images of the galaxy had to do with the presence of the young stars. In order to solve this problem, we had to introduce the distribution of the young stars as a separate component in the model. Our first guess was to use a second exponential (in both R and z directions) disk. It turned out that the radial scalelength of this second disk was huge. Thus we approximated the second disk (hereafter young stellar disk) as being constant in the radial directions. The emissivity this disk is distributed exponentially in the vertical direction and is constant in the radial direction, truncated at the visual end of the galaxy, namely

$$L_{OB}(R,z) = \begin{cases} L_{OB} \exp\left(-|z|/z_{OB}\right) & , \; R \leq R_{OB} \\ 0 & , \; R > R_{OB} \end{cases} \quad (9)$$

with L_{OB} being the emissivity of this disk at the center of the galaxy and z_{OB} the scaleheight of this disk. Here R_{OB} is the truncation radius of this disk which was taken to be approximately equal to the visual radius of the galaxy ($\sim$ 14 kpc). The central surface brightness for this model disk, if it is seen edge-on, is

$$I_{OB} = 2 L_{OB} R_{OB}. \quad (10)$$

Although the young stars seem to be distributed in a more clumpy and non-symmetric way, which probably has to do with

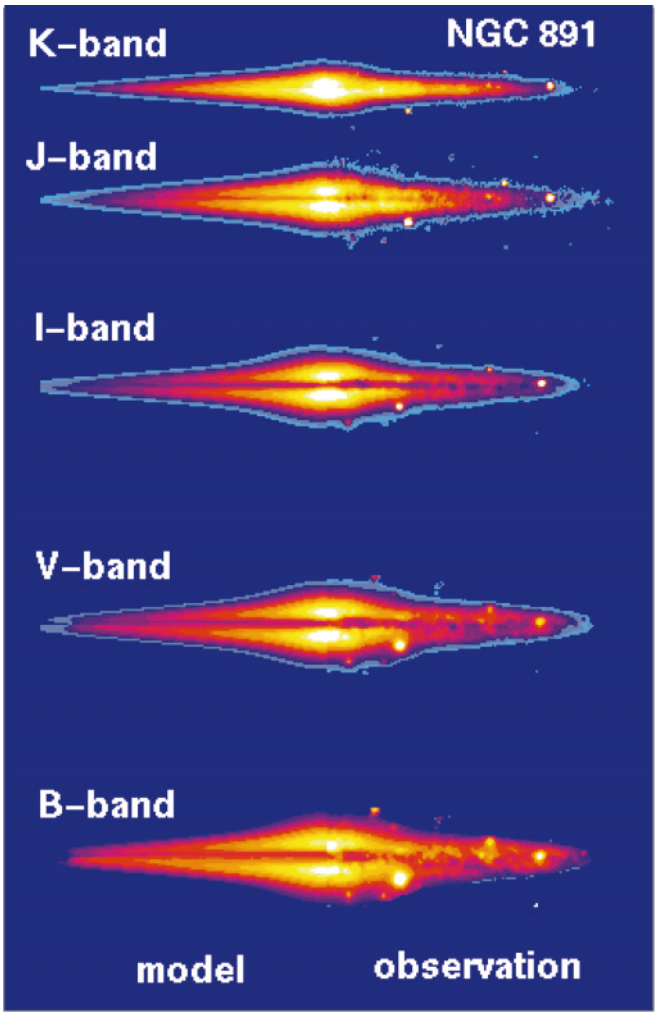

Fig. 3. Images of NGC 891 in K, J, I, V, B bands (top to bottom). The left half in each panel is the model image and the right half is the real galaxy image (folded).

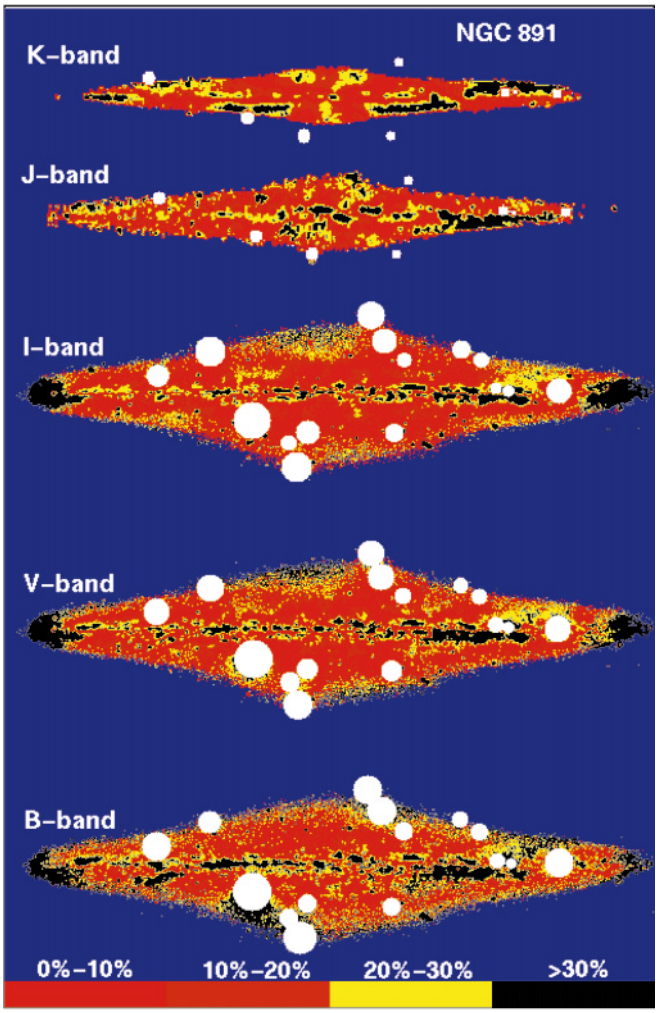

Fig. 4. Colour map, showing the absolute relative error between the observed images and the model images in the K, J, I, V, B bands (top to bottom). See text for a detailed description.

the spiral structure, this disk approximately takes account of the extra light coming from the young stars and gives reasonable fits to the observed data (see below). Adding the new disk, the total stellar emissivity becomes

$$L(R,z) = L_{disk}(R,z) + L_{OB}(R,z) + L_{bulge}(R,z). \quad (11)$$

With the new distributions we run the model again in all five bands (B, V, I, J, K). Besides the parameters of the fit that were used before, two more parameters have been added (I_{OB} and z_{OB}). The young stellar disk that we included in the model was only detected in the V and B bands. In the other bands (I, J, K) this disk was not detected, in the sense that the values derived for the central luminosity density were very small positive or negative values with errors much larger than the values themselves and with all the other parameters taking values very similar to those presented in Table 1. This suggests that in these bands the contribution of the young stars is not important compared to the stars in the main disk of the galaxy. This is also evident just by visual inspection of the galaxy image in all bands. The values derived from the fit for the B and V bands are given in Table 2. Comparing the values for the common parameters given in Tables 1 and 2 for the B and V models, we see that all of them are very similar. This means that the young stellar disk that was included in the model, appears able to account for the light coming from the young stars, so that the rest of the galaxy can be very well described by the ten parameter model, the results of which are given in Table 1.

5. Conclusions

Having derived the parameters that best describe the galaxy in all bands, we have created model images and compare them with the real observations. We do so in Fig. 3 where the 2D image of NGC 891 in the K, J, I, V and B bands (top to bottom) is presented, with the model in the left half of the frame and the folded real galaxy in the right half of each panel. In Fig. 4 we show the absolute value of the residuals between the observed galaxy and the model galaxy that we produced. These maps show how

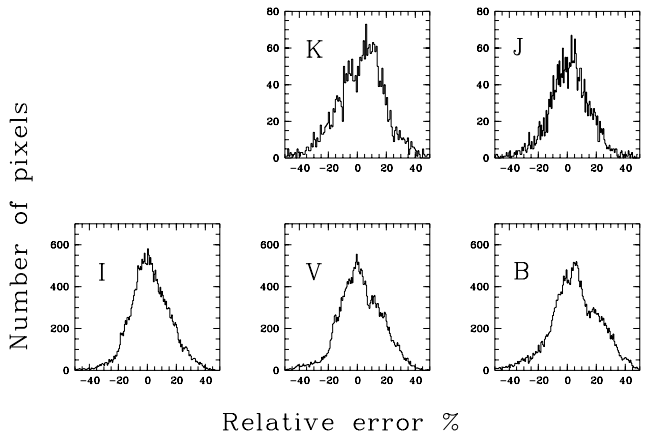

Fig. 5. Histograms of the relative errors between the real folded image of the galaxy and the model image.

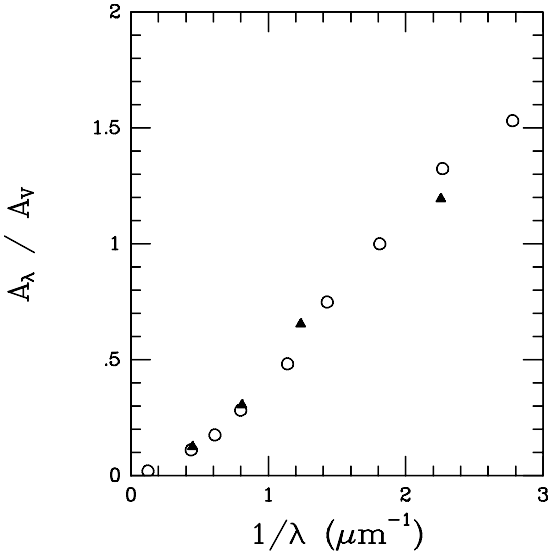

Fig. 6. The observed (open circles) values of A_λ/A_V for our Galaxy and the values calculated from the model (solid triangles) for NGC 891.

these residuals are distributed throughout the galaxy's image in terms of the absolute value of the percentage error. Red corresponds to areas with error less than 10%, orange corresponds to areas with error between 10% and 20%, yellow corresponds to areas with error between 20% and 30% and black corresponds to areas with error greater than 30%. White circles indicate the positions of the brightest foreground stars. In Table 3 we give the statistics derived from the residual maps shown in Fig. 4. In this table we give the percentage of the galaxy's image in each filter with residuals less than 10%, 20%, 30%, 40% and 50%. We see that on average, almost 70% of the total galaxy's image has residuals less than 20%, while 90% of the image is with residuals less than 40%.

The goodness of the fit of our model to the real data is also seen in Fig. 5, where the histograms of the relative errors between the model galaxy image and the observed *folded* galaxy image are given for the five bands modelled. These histograms show a quite symmetrical distribution of the relative errors between positive and negative values. This means that the global fit that was done to the observed image of the galaxy accomplished the highest possible match between the smooth distribution given by the model and the real data with all the clumpiness and non-uniform structure that they have.

An important result is that the dust is found to be extended in the radial direction, giving a scalelength which on average is 1.5 times larger than that of the stars. In the other (vertical) direction, the dust is concentrated in the central plane, with a scaleheight of about 1.5 times less than that of the stars. The value of 0.15 kpc obtained for the scaleheight of the young stars, is in good agreement with the scaleheight of the OB stars determined for our Galaxy (Wainscoat et al. 1992, Corradi et al. 1996) which is in the range of 0.09 - 0.11 kpc. In the K-band, we see a drop of the scaleheight of the stars to the value of 0.32 kpc, indicating a thinner stellar disk in these wavelengths, or maybe a departure from the exponential form. This is also evident in Fig. 4, where areas with high residuals are distributed symmetrically in the disk.

The filter that was used for the data modelled in KB87 was an IIIa-F emulsion filter with approximate range in wavelengths 0.58 - 0.69 μm. This puts it somewhere between the V and I passbands that we use in this study. Some of the values derived for the disk parameters in KB87 can be compared and are in good agreement with the mean values between V and I bands that have been derived in this study. For the scalelengths of the stars and the dust for example, where in both studies exponential radial distributions were used, we find a mean value of 5.1 kpc for the scalelength of the stars, while 4.9 kpc was found in KB87. For the scalelength of the dust, we found 7.5 kpc while in KB87 this parameter was not determined but it was estimated to be in the range 3.9 - 7.3 kpc. For the scaleheights of the stars and the dust though, we can not compare between the two studies since in this study we use an exponential distribution in z, while a sech^{2}z law was used in KB87. For the central face-on optical depth, we found 0.60, while a value of 0.46 was found in KB87. This difference is mainly due to two reasons. First, the exponential distribution in the z-direction provides an upper limit to the central optical depth, because near the center of the galaxy this function is steeper than the sech^{2}z law allowing for more dust. On the other hand, the bulge component that was added in this study, but was not taken into account in KB87, produced extra light and as a result more dust had to be added in order to absorb this extra light.

Dust and gas mass calculations for NGC 891 have been reported in Devereux & Young (1990). Assuming a distance of 14.1 Mpc for this galaxy (as opposed to 9.5 Mpc assumed by us) and using the IRAS 60μm and 100μm fluxes, the authors derive a dust mass of 1.90×10^7 $M_\odot$. For the same galaxy, the gas mass was found to be 1.82×10^{10} $M_\odot$, resulting in a gas to dust mass ratio of 940. Using the results derived from our model (given in Table 1) and scaling them to the distance of 14.1 Mpc, we can calculate the total dust mass in the galaxy.

The formulae that we have used are given in Sect. 5.3 of Paper I. With these calculations, the dust mass derived from the model is $1.10 \times 10^8\ M_\odot$. Using this value, the gas to dust mass ratio becomes

$$\frac{M_g}{M_d} = 165 \tag{12}$$

which is very close to the value of 167 adopted for our Galaxy (Spitzer 1987, p.162) and also the value of 121 derived for UGC 2048 in Paper I. The dust mass derived from our model, is higher than the dust mass calculated using the IRAS fluxes. This is to be expected, because cold dust also exists, and has gone undetected by IRAS which only measures the warm dust. Our calculations are also supported by the 1.3 mm emission measured by IRAM (Guélin et al. 1993) which is nine times stronger than that predicted by the IRAS "warm dust" contribution.

From the face-on central optical depth of the dust $\tau_\lambda^f = 2\kappa_\lambda z_d$ and given a mean value for the scaleheight of the dust z_d = 0.26 kpc for all the filters, we calculate the absorption coefficient κ_λ in each band. We have found that κ_B/κ_V = 1.194, κ_I/κ_V = 0.653, κ_J/κ_V = 0.305 and κ_K/κ_V = 0.125. These values are directly compared to the ratio of the extinction values A_λ/A_V and are plotted as a function of the effective wavelength in Fig. 6. Solid triangles correspond to the values derived with our model, while open circles are the values given by Rieke & Lebofsky (1985) for our Galaxy.

6. Summary

Using a three dimensional axisymmetric model of stars and dust in NGC 891, we have been able to determine all the parameters that best describe the distribution of stars and dust in this galaxy in the optical and NIR bands.

We have found that NGC 891 would be *optically thin* in this range of wavelengths if it was to be seen face-on. For the characteristic scales of the galaxy we find : $z_s \approx 0.4$ kpc, $z_d \approx 0.26$ kpc, $h_s \approx 4-6$ kpc (from K to B) and $h_d \approx 8$ kpc. A second stellar disk with a scaleheight of 0.15 kpc is invoked to describe the young stellar population which is easily seen in this galaxy.

The dust mass calculations as well as the extinction law derived with our model, confirm that NGC 891 is a galaxy very similar to our own.

Acknowledgements. We thank Dr. R.L.M. Corradi for his useful comments. We are also grateful to M. Woche and E. Paleologou for their help in the optical observations and Harley Thronson, Norbert Pirzkal and Brenae Baily for their help in obtaining the NIR observations. This research has been supported in part by a Greek-British Joint Research Program and by a P.EN.E.D. Program of the General Secretariat of Research and Technology of Greece. Skinakas Observatory is a collaborative project of the University of Crete, the Foundation for Research and Technology-Hellas and the Max-Planck-Institut für Extraterrestrische Physik.

References

Alton P.B., Davies J.I., Trewhella M., 1997, MNRAS, (submitted)
Aaronson M., 1977, Ph.D. thesis, Harvard University
Bahcall J.N, Kylafis N.D., 1985, ApJ, 288, 252
Bruzual G.A., Magris G.C., Calvet N., 1988, ApJ, 333, 673
Corradi R.L.M., Beckman J.E., Simonneau E., 1996, MNRAS, 282, 1005
de Vaucouleurs G., 1953, MNRAS, 113, 134
Devereux N.A., Young J.S., 1990, ApJ, 359, 42
Guélin M., Zylka R., Mezger P.G., et al., 1993, A&A, 279, L37
Henyey L.G., Greenstein J.L., 1941, ApJ, 93, 70
Hubble E.P., 1930, ApJ, 71, 231
Kylafis N.D., Bahcall J.N, 1987, ApJ, 317, 637
Rieke G.H., Lebofsky M.J., 1985, ApJ, 288, 618
Shaw M.A., Gilmore G., 1989, MNRAS, 237, 903
Spitzer L., 1978, Physical Processes in the Interstellar Medium, New York, Wiley-Interscience
van der Kruit P.C., Searle L., 1981, A&A, 95, 116
Wainscoat R.J., de Jong T., Wesselius P.R., 1987, A&A, 181, 225
Wainscoat R.J., Cohen M., Volk K., Walker H., Schwartz D.E., 1992, ApJS, 83, 111
Xilouris E.M., Kylafis N.D., Papamastorakis J., Paleologou E.V., Haerendel G., 1997, A&A, 325, 135

This article was processed by the author using Springer-Verlag LaTeX A&A style file *L-AA* version 3.